


RESEARCH

Open Access



Evaluating the impact of sampling schemes on leaf area index measurements from digital hemispherical photography in *Larix principis-rupprechtii* forest plots

Jie Zou^{1,2*} , Wei Hou^{1,2}, Ling Chen³, Qianfeng Wang⁴, Peihong Zhong^{1,2}, Yong Zuo^{1,2}, Shezhou Luo⁵ and Peng Leng^{1,2}

Abstract

Background: Digital hemispherical photography (DHP) is widely used to estimate the leaf area index (LAI) of forest plots due to its advantages of high efficiency and low cost. A crucial step in the LAI estimation of forest plots via DHP is choosing a sampling scheme. However, various sampling schemes involving DHP have been used for the LAI estimation of forest plots. To date, the impact of sampling schemes on LAI estimation from DHP has not been comprehensively investigated.

Methods: In this study, 13 commonly used sampling schemes which belong to five sampling types (i.e. dispersed, square, cross, transect and circle) were adopted in the LAI estimation of five *Larix principis-rupprechtii* plots (25 m × 25 m). An additional sampling scheme (with a sample size of 89) was generated on the basis of all the sample points of the 13 sampling schemes. Three typical inversion models and four canopy element clumping index (Ω_e) algorithms were involved in the LAI estimation. The impacts of the sampling schemes on four variables, including gap fraction, Ω_e , effective plant area index (PAI_e) and LAI estimation from DHP were analysed. The LAI estimates obtained with different sampling schemes were then compared with those obtained from litter collection measurements.

Results: Large differences were observed for all four variable estimates (i.e. gap fraction, Ω_e , PAI_e and LAI) under different sampling schemes. The differences in impact of sampling schemes on LAI estimation were not obvious for the three inversion models, if the four Ω_e algorithms, except for the traditional gap-size analysis algorithm were adopted in the estimation. The accuracy of LAI estimation was not always improved with an increase in sample size. Moreover, results indicated that with the appropriate inversion model, Ω_e algorithm and sampling scheme, the maximum estimation error of DHP-estimated LAI at elementary sampling unit can be less than 20%, which is required by the global climate observing system, except in forest plots with extremely large LAI values ($\sim > 6.0$). However, obtaining an LAI from DHP with an estimation error lower than 5% is impossible regardless of which combination of inversion model, Ω_e algorithm and sampling scheme is used.

(Continued on next page)

* Correspondence: zoujie@fzu.edu.cn

¹The Academy of Digital China (Fujian), Fuzhou University, Fuzhou 350116, China

²Key Laboratory of Data Mining and Information Sharing, Ministry of Education, Fuzhou 350116, China

Full list of author information is available at the end of the article



© The Author(s). 2020 **Open Access** This article is licensed under a Creative Commons Attribution 4.0 International License, which permits use, sharing, adaptation, distribution and reproduction in any medium or format, as long as you give appropriate credit to the original author(s) and the source, provide a link to the Creative Commons licence, and indicate if changes were made. The images or other third party material in this article are included in the article's Creative Commons licence, unless indicated otherwise in a credit line to the material. If material is not included in the article's Creative Commons licence and your intended use is not permitted by statutory regulation or exceeds the permitted use, you will need to obtain permission directly from the copyright holder. To view a copy of this licence, visit <http://creativecommons.org/licenses/by/4.0/>.

(Continued from previous page)

Conclusion: The LAI estimation of *L. principis-rupprechtii* forests from DHP was largely affected by the sampling schemes adopted in the estimation. Thus, the sampling scheme should be seriously considered in the LAI estimation. One square and two transect sampling schemes (with sample sizes ranging from 3 to 9) were recommended to be used to estimate the LAI of *L. principis-rupprechtii* forests with the smallest mean relative error (MRE). By contrast, three cross and one dispersed sampling schemes were identified to provide LAI estimates with relatively large MREs.

Keywords: Sampling scheme, Elementary sampling unit, Clumping index, Leaf area index, Digital hemispherical photography, Forest, *Larix*

Introduction

Leaf area index (LAI) is an important forest structure parameter that is defined as one half of the total canopy element green area per unit ground area of forest plots (Watson 1947; Chen and Black 1992). LAI is required in most forest biophysical and physiological process models (Running and Hunt 1993; Zou et al. 2018b). It can be measured at the elementary sampling unit (ESU) scale via direct or indirect methods, and can be retrieved from remote sensing images at the regional, national or even global scale. ESU-scale LAI estimates are typically used to evaluate satellite-derived LAI products due to their relatively high accuracies and reliabilities.

LAI is one of the 16 essential terrestrial climate variables required by the global climate observing system (GCOS). GCOS has specified that the estimation error of LAI products must be limited to 20% and should be improved to 5% for future applications (Fernandes et al. 2014; Woodgate 2015). However, large differences have been reported amongst commonly used LAI products (Garrigues et al. 2008; Fang et al. 2013; Chen 2014). Therefore, accurate ESU-scale LAI estimates are required to consistently evaluate LAI products in order to pick out qualified LAI products and improve those unqualified ones.

Optical methods are typical indirect methods to obtain the ESU LAI of forests with high efficiency and low cost (Jonckheere et al. 2004; Zou et al. 2009), including LAI-2000/LAI-2200 (LI-COR, Lincoln, NE, USA), digital hemispherical photography (DHP) (Jonckheere et al. 2004; Weiss et al. 2004), multiband canopy imaging methods such as multiband vegetation imager (Zou et al. 2009) and multispectral canopy imager (Kucharik et al. 1997), as well as the tracing radiation of canopy and architecture method (3rd Wave Engineering, Winnipeg, Manitoba, Canada) (Leblanc and Chen 2002). Previous studies reported that the LAI estimation error of optical methods in the ESU LAI estimation of forests are mainly caused by inversion models (Liu et al. 2015; Zou et al. 2018b), clumping effects (Leblanc and Chen 2002; Leblanc et al. 2005; Chen et al. 2006; Zou et al. 2018b), nonphotosynthetic components (Weiss et al. 2004; Zou et al. 2009; Ercanlı et al. 2018; Zou et al. 2018a), terrain slopes (Gonsamo and

Pellikka 2008; Cao et al. 2015), sampling schemes (Nackaerts et al. 2000; Weiss et al. 2004; Majasalmi et al. 2012; Pfeifer et al. 2018) and observation conditions (Leblanc and Chen 2001; Jonckheere et al. 2004; Zhang et al. 2005). In recent years, great efforts have been made to reduce the ESU LAI estimation errors of optical methods, and numerous advancements have been achieved through the involvement of appropriate inversion models (Leblanc and Fournier 2014; Woodgate 2015; Zou et al. 2018b), terrain slope correction methods (Cao et al. 2015) and woody components (nonphotosynthetic components) correction methods (Zou et al. 2018a; Zou et al. 2019). However, to the best of our knowledge, no attempt has been made to evaluate the impact of sampling schemes on the ESU LAI estimation of forests via optical methods. Sampling schemes with various numbers and spatial arrangements of sample points have been adopted by optical methods such as DHP and LAI-2000/LAI-2200, to estimate the ESU effective plant area index (PAI_e), effective woody area index and LAI of forest plots. For example, sample points were spatially arranged in certain patterns such as circle (Soto-Berelov et al. 2015; Woodgate 2015), square (Neumann et al. 1989; Baret et al. 2005; Macfarlane et al. 2007; Ryu et al. 2010a; Pisek et al. 2011; Woodgate et al. 2012; Liu et al. 2015), transect (Cutini et al. 1998; van Gardingen et al. 1999; Hyer and Goetz 2004; Abuelgasim et al. 2006; Ryu et al. 2010a; Majasalmi et al. 2012), cross (Leblanc 2008; Woodgate et al. 2012; Leblanc and Fournier 2014; Zou et al. 2018a) and dispersed (Abuelgasim et al. 2006; Majasalmi et al. 2012). Moreover, different sample sizes ranging from 1 to 176 have been applied at the ESU scale (Cutini et al. 1998; van Gardingen et al. 1999; Nackaerts et al. 2000; Macfarlane et al. 2007; Gonsamo et al. 2010; Ryu et al. 2010a; Pisek et al. 2011; Woodgate 2015; Calders et al. 2018; Zou et al. 2018a; Zou et al. 2018b).

Previous studies have reported obvious differences in the PAI_e estimates from different sampling schemes (Nackaerts et al. 2000; Majasalmi et al. 2012; Calders et al. 2018). Similar to the PAI_e obtained indirectly from

gap fraction measurements, canopy element clumping index (Ω_e), which can be estimated by current available algorithms such as gap-size analysis (CC) (Chen and Cihlar 1995a), finite-length averaging (LX) (Lang and Yueqin 1986) and combination of gap-size and finite-length averaging (CLX) (Leblanc et al. 2005), also depends on gap fraction and gap size measurements from the optical method. Therefore, Ω_e estimation should also be affected by sampling schemes.

Different zenith angles (θ) have been used by different inversion models. For instance, the effective zenith angle range for the Nilson model (Nilson 1999) and the Miller theorem (Miller) (Miller 1967) is from 0° to 90° , while the zenith angle range for the LAI calculation method of the LAI-2200 instrument is from 0° to 74° (LAI-2200) (LI-COR 2009), and zenith angles near 57.3° are used for Beer's law (Beer) (Ross 1981; Leblanc and Fournier 2014; Zou et al. 2018b). Variations in gap fraction or Ω_e measurements with zenith angles ranging from 0° to 90° are usually large for forest plots (Leblanc et al. 2005; Liu et al. 2015; Woodgate 2015; Zou et al. 2018b). Therefore, LAI estimation is expected to be influenced by inversion models which depend on gap fraction and Ω_e measurements. For example, the plant area index (PAI) estimates of forest plots were reported to be largely affected by inversion models (Zou et al. 2018b). Therefore, accurate ESU-scale LAI should be obtained by the joint consideration of inversion models, Ω_e algorithms and sampling schemes.

The following three aspects of sampling schemes need further investigation to improve LAI estimates from DHP. First, the PAI_e estimated from DHP is 35%–75% of the PAI of forest canopies if Ω_e is ignored in the estimation (Leblanc and Chen 2002; Zou et al. 2018b). Therefore, the impact of sampling schemes on PAI estimates should be started by investigating the impact of sampling schemes on Ω_e estimation. However, no attention has been paid to such impact yet. Second, large differences were observed in the PAI or LAI of the same forest plot obtained from optical methods with different inversion models (Ryu et al. 2010a; Zou et al. 2018a; Zou et al. 2018b). However, only one inversion model (i.e. Beer or LAI-2200) was used to evaluate the impact of sampling schemes on the PAI_e estimation of forest plots (Nackaerts et al. 2000; Majasalmi et al. 2012; Calders et al. 2018). Thus, whether the impact of sampling schemes on LAI estimation varies with different inversion models should be investigated. Third, recommendations should be given to select optimal sampling schemes for accurate ESU LAI estimation of forests.

In this study, DHP images were collected at 89 unique sample points of 13 sampling schemes in five typical *Larix principis-rupprechtii* forest plots. Three commonly used inversion models (i.e. Miller, LAI-2200 and Beer)

and Ω_e estimation algorithms (i.e. CC, LX and CLX) were adopted to estimate the ESU LAI of forests. The main purposes of this study are to: (1) analyse the impact of sampling schemes on gap fraction, Ω_e , PAI_e and LAI estimations; (2) evaluate the performance of sampling schemes on the ESU LAI estimation of forests using litter collection LAI measurements; and (3) identify the best sampling scheme for the ESU LAI estimation of forests.

Theory

The LAI of forest canopies can be obtained on the basis of the PAI from DHP and woody-to-total area ratio (α) measurements:

$$\text{LAI} = \text{PAI} \times (1 - \alpha). \quad (1)$$

In the current study, three models (i.e. Miller, LAI-2200 and Beer) were used because they were reported to outperform other commonly used inversion models in the PAI estimation of forest canopies (Zou et al. 2018b). Several algorithms have been proposed to estimate the Ω_e of forest canopies using gap fraction or gap size measurements collected from DHP. They include CC, LX, CLX, modified gap-size analysis (Pisek et al. 2011), modified finite-length averaging (Gonsamo and Pellikka 2009) and Pielou's coefficient of spatial segregation (Walter et al. 2003). Pielou's coefficient of spatial segregation algorithm was claimed to produce inaccurate Ω_e estimates (Walter et al. 2003; Pisek et al. 2011; Zou et al. 2018b). High similarities were found between CC and modified gap-size analysis as well as between LX and modified finite-length averaging algorithms (Zou et al. 2018b). Moreover, amongst CC, LX and CLX, no single algorithm is better than the other two in the Ω_e estimation of all forest plots (Zou et al. 2018b). Therefore, all three algorithms (i.e. CC, LX and CLX) were adopted in the PAI estimation in this study. The details of the formula to obtain the Ω_e and PAI of forest plots can be found in Additional file 1.

Materials and methods

Plot description

The study area is located in the Saihanba National Forest Park in Hebei Province, China. Five even-aged plots of $25\text{ m} \times 25\text{ m}$ (ESU) that covered typical ages of *L. principis-rupprechtii* in the study area were used. *L. principis-rupprechtii* is one of the dominant and widespread tree species in northern China. The five plots are at least about 120 m away from the forest border. The structure characteristics of the canopy around the plots are similar to those of the plots. The majority of branches below the live canopy in plot 1 and 2 were harvested by local forest managers before our field

experiment. Dead branches at heights below 2.5 m in plots 3 and 4 were harvested in the low and medium levels before the field campaign (Zou et al. 2018a). The main characteristics of the five plots are listed in Table 1.

Data acquisition and processing

DHP

Thirteen sampling schemes (SS1–SS13) (predefined sampling schemes) comprising 89 unique sample points were used in this study (Fig. 1). Figures 1a–d show four square sampling schemes, amongst which 9, 16 and 25 sample points were evenly distributed in the plots for SS2, SS3 and SS4, respectively. Figures 1e–g show three cross sampling schemes (i.e. SS5, SS6 and SS7), amongst which the sample points were located at or close to the two perpendicular centre lines of each plot. Compared with SS6, one additional sampling point was added in each quadrant 2.5 m away from the centre lines for SS7 to increase the canopy sampling of the centre areas of the plots (Leblanc 2008). Two dispersed sampling schemes are shown in Fig. 1h and i. For SS8, three sample points were randomly distributed within the plot along with one central point and eight others were distributed evenly on the boundary lines. For SS9, four sample points were distributed evenly along one of the diagonal lines and 12 sample points were distributed evenly on the four boundary lines. Figure 1j–l illustrate three transect sampling schemes, in which sample points were evenly distributed along the diagonal lines. A total of 13 sample points in a circle sampling scheme (i.e. SS13) were evenly distributed with a distance interval of 5 m along three intersecting lines with the same intersection angle of 60° (Woodgate 2015). The number of sample points for these 13 sampling schemes ranged from 3 (i.e. SS10) to 25 (i.e. SS4). To increase the number of sample points, a sampling scheme (SS14) (simulated sampling scheme) was generated using all the sample points

from these 13 sampling schemes to represent the sample scheme with 89 sample points (Fig. 1n). For SS14, the distances between the neighbour points for all sampling points ranged from 0.7 to 5.9 m (Fig. 1n). The position of each sampling point of all sampling schemes in the field was established with tape and marked with wooden stakes with flags to facilitate the DHP image collection (Zou et al. 2018a). Parts of the 89 sampling points were slightly moved from its designed positions to new adjacent positions in the field in order to make the positions of all sampling points were at least about 0.6 m away from its nearest large tree stems. This movement is necessary in order to avoid the greatly increased visible proportion of stems in DHP images.

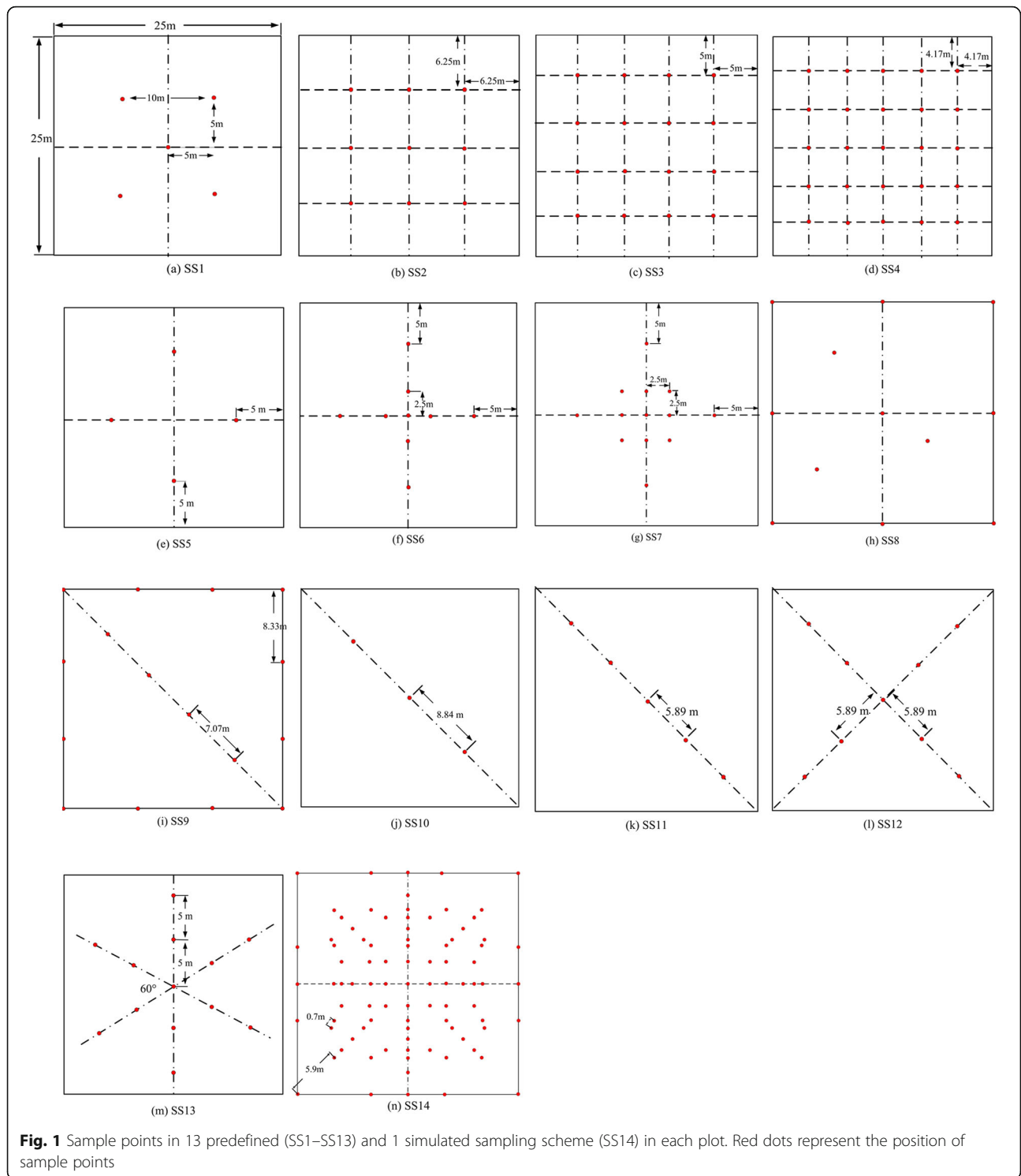
DHP images were collected using a Canon 6D camera with a Sigma 8 mm fisheye lens before sunrise, after sunset or under overcast conditions (Zou et al. 2018a). The DHP image resolution was 5472 × 3648 pixels. Manual exposure mode was used in the DHP image collection. The exposure was determined using the method described in Leblanc et al. (2005) and Woodgate et al. (2015) to achieve good contrast between canopy element and sky. The camera was set approximately 1.2 m above the ground. The DHP images were acquired one by one at all 89 unique sample points of the 13 sampling schemes in each plot. A total of 445 DHP images were obtained from the five plots. The DHP images were taken in 2017 from August 11 to September 2, which was the peak season with maximum LAI of the year for the five plots (Zou et al. 2018a; Zou et al. 2019).

The DHP images were manually processed using Adobe Photoshop 7.0 (Adobe Systems, San Jose, CA, USA). The image preprocessing procedures included image cropping, blue channel selection, gamma correction (the gamma of the blue channel was corrected to about 1.0) and image classification (Gonsamo and

Table 1 Characteristics of the *Larix principis-rupprechtii* plots (Zou et al. 2018a)

| | Plot 1 | Plot 2 | Plot 3 | Plot 4 | Plot 5 |
|---|--------------------------|--------------------------|-------------------------|---------------------------|---------------------------|
| Longitude and latitude | 42°24'43" N, 117°19'4" E | 42°24'2" N, 117°18'40" E | 42°18'2" N, 117°18'9" E | 42°25'22" N, 117°19'32" E | 42°17'42" N, 117°16'53" E |
| Mean tree height (m) | 19.43 | 20.4 | 12.58 | 13.31 | 8.73 |
| Average DBH ^a (cm) | 26.58 | 27.22 | 12.71 | 14.14 | 9.23 |
| Stand density (stems·ha ⁻¹) | 464 | 384 | 2320 | 1760 | 3904 |
| Tree age (~yrs) | 54 | 55 | 21 | 22 | 13 |
| Needle-to-shoot area ratio | 1.30 | 1.17 | 1.14 | 1.17 | 1.28 |
| Woody-to-total area ratio | 0.16 | 0.16 | 0.20 | 0.24 | 0.23 |
| Litter collection LAI | 4.65 | 3.58 | 4.96 | 3.04 | 6.69 |
| Slope | ~ 0° | | | | |

^aDiameter at breast height



Pellikka 2008; Zou et al. 2018a). The threshold values for the DHP images to be classified into canopy element and sky were determined by referring to the mean digital numbers of the canopy element and sky peaks in the histogram of the blue channel images.

In this study, a narrow zenith angle range of 52°–62° was used by the Beer inversion model. Segment size is a key parameter required by LX and CLX in Ω_e estimation. This parameter was used to divide each annulus of DHP into several small segments and make the canopy

element at the segment scale approach random spatial distribution which was assumed by LX. The 5° segment size recommended by Gonsamo et al. (2010) was adopted for LX (hereinafter, LX_5, in which '5' represents the segment size of 5°); this size would result in 72 segments for each annulus of DHP. As for CLX, no large differences were found between the root mean square error and mean absolute error of the PAI of forest plots estimated using the same inversion model and CLX but with three segment sizes of 15°, 30° and 45° (Zou et al. 2018b). Therefore, for simplicity, only the 15° segment size was chosen for CLX (CLX_15) to calculate Ω_e in this study. For CC, two transect processing schemes (i.e. CCW and CCS) were used in the Ω_e estimation. CCW merges the transects of all DHP images into a whole transect to calculate the Ω_e for each sampling scheme. By contrast, CCS treats the transect of each DHP image individually and the final Ω_e is obtained by averaging the Ω_e of all DHP images for each sampling scheme. The same estimation procedure to obtain Ω_e at zenith angles ranging from 0° to 90° with a 1° interval, as suggested by our previous study (Zou et al. 2018b), was also used in the current study. MTVSP software (version 2018) (Zou et al. 2015; Zou et al. 2018a) was operated to estimate the canopy element gap fraction at θ ($p_e(\theta)$), Ω_e , PAI_e, PAI and LAI of the five plots from the preprocessed DHP images. PAI_e and PAI of each plot were calculated using the mean $p_e(\theta)$ of all processed DHP images of each sampling scheme, as suggested by Ryu et al. (2010b). For each sampling scheme of each plot, 3 PAI estimates were calculated using Equations A6–A8 on the basis of the $p_e(\theta)$, canopy element gap fraction of the *i*th annulus of LAI-2200 (p_{e_i}), canopy element gap fraction at 57° ($p_e(57)$) and Ω_e estimate, which was obtained from one Ω_e algorithm amongst the four Ω_e algorithms (i.e., CCS, CCW, LX_5 and CLX_15). Then 12 PAI estimates were obtained for each sampling scheme of each plot. Next, 12 LAI estimates were calculated for each sampling scheme of each plot using Equation (1) based on the calculated PAI and α measurements, which were obtained with destructive measurements (detailedly described in section below).

The $p_e(\theta)$ measurements of annuli with zenith angles close to 90° were tended to approach or equal to zero. In this study, PAI or LAI under the condition of zero gap fraction was defined as 10 (Zou et al. 2018b). The upper limit of the estimated LAI for very small $p_e(\theta)$ measurements was set to 10 to avoid obtaining unrealistically high LAI estimates (Leblanc et al. 2005; Pisek et al. 2011; Yan et al. 2019).

α , γ and LAI

The α for each plot was estimated with destructive measurements of two or three representative trees that were

selected and harvested. The stems and branches of the harvested trees were divided into height classes with a height interval of 1 m and a starting height of 1.2 m. The stem, branch and fruit areas of each height class for each harvested tree were measured with a tape or a digital calliper, with the assumption that the stem or branch sections were circular truncated cones and the fruits were spheroids (Zou et al. 2018a). Approximately 300–350 typical needles were randomly selected from the branches of each height class or several height classes with similar needle characteristics. The needle cross section was assumed to be rectangular in shape. The hemisurface area of typical needles was measured with the volume displacement method described by Chen et al. (1997). The dry mass of typical needles and all needles of each height class of each tree were obtained by drying the needles at 65 °C for 48 h until the weights of the needles remained almost unchanged. For these typical needles, the specific leaf area was obtained by dividing the hemisurface area by the dry mass. The leaf area of a height class was calculated by multiplying the specific leaf area with the dry mass of all needles in that height class. The leaf area of each harvested tree was the sum of the leaf area of every height class for that tree. The α of each harvested tree was then calculated by dividing the area of the woody components (stem, branches and fruits) by the sum of the woody components and leaf areas of that tree. The α of each plot was calculated using the α of the representative trees and the DBH measurements of each plot. Details of the α estimation of the five plots are available in our previous work (Zou et al. 2018a).

For each plot, two to four typical shoots were randomly selected from each height class of forest canopy (i.e. bottom, middle and top) for needle-to-shoot area ratio (γ) determination. Incomplete and abnormal (untypical) shoots were discarded before the estimation of γ . For each typical shoot, the projection areas were recorded using a Canon 6D camera equipped with a Canon 24–70 mm lens and a flat, levelled white panel with two rulers laid on its top surface (Zou et al. 2018a). Three shoot projection images were taken right above each shoot sample at a distance of approximately 0.6 m by rotating the shoot main axis to three zenith angles (i.e. 0°, 45° and 90°) and one azimuth angle (i.e. 0°). Afterwards, the three projection areas of the typical shoot ($A_p(0^\circ, 0^\circ)$, $A_p(45^\circ, 0^\circ)$ and $A_p(90^\circ, 0^\circ)$) were calculated according to the three shoot projection images (Zou et al. 2018a). The half of the total needle area in a typical shoot (A_n) was measured by the volume displacement method described by Chen et al. (1997). Then, the effective needle-to-shoot area ratio (γ_e) of each shoot could be obtained with Equation (A1). The γ_e of each plot was obtained by averaging the γ_e of all typical

shoots. Then the γ of each plot was obtained with Equation (A2) on the basis of γ_e and α .

In each plot, nine litter traps of 50 cm × 50 cm in size were placed 50 cm aboveground at each sample point of SS2. The litter collection was started before defoliation and ended after it. The measurements

were performed six times during the entire period, on September 1, 18 and 29 and October 13, 18 and 24 in each plot. During each measurement time, approximately 300–350 typical needles were randomly selected from the litter collections of each plot to measure the specific leaf area. The method for the

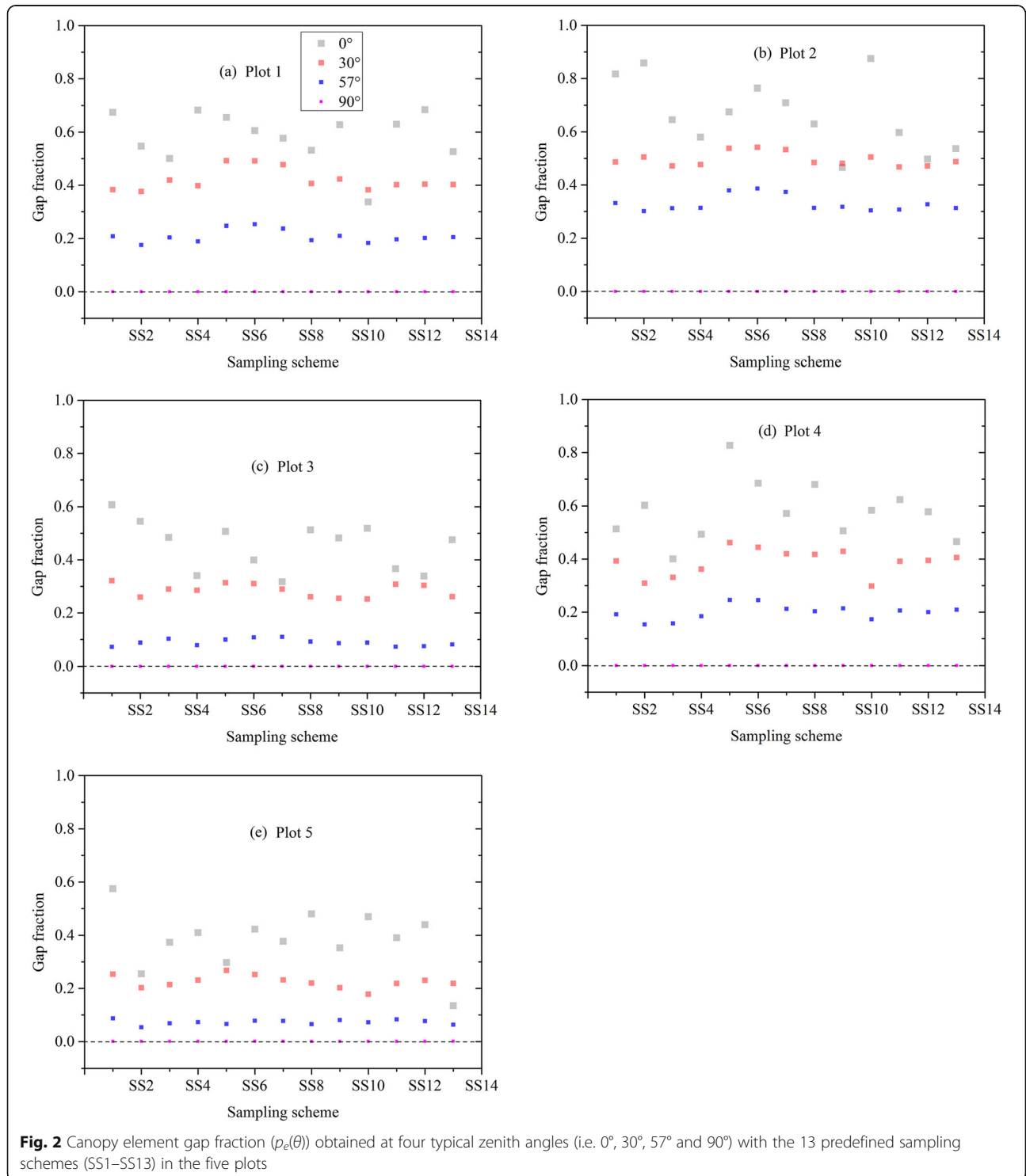


Fig. 2 Canopy element gap fraction ($p_e(\theta)$) obtained at four typical zenith angles (i.e. 0°, 30°, 57° and 90°) with the 13 predefined sampling schemes (SS1–SS13) in the five plots

calculating the specific leaf area of the typical needles was the same as those for calculating α . The dry mass of all needles of each measurement time for each plot was obtained by drying the needles at 65 °C for 48 h until the weights of the needles remained almost unchanged. Totally six specific leaf area and dry mass measurements corresponding to the six measurement times, respectively, were obtained for each plot. In each plot, the one-half of the area of fallen needles for each measurement time was obtained by multiplying the specific leaf area by the dry mass of all fallen needles of that measurement time. The LAI of each plot was then obtained by dividing one-half of the total area of the fallen needles collected during the six measurement times by the area of the litter traps.

Statistical analysis

Mean relative error (MRE), which is similar to the mean relative deviation from Calders et al. (2018), was used in this study because it corresponds to the accuracy

evaluation required by GCOS. The MRE of the LAI for each combination of inversion model, Ω_e algorithm and sampling scheme was calculated using the litter collection LAI as the reference.

Results

Effect of sampling schemes on gap fraction ($p_e(\theta)$) estimation

Obvious differences were observed amongst the $p_e(\theta)$ from different predefined sampling schemes at the four typical zenith angles, except at 90°, and the differences seem to decrease with the zenith angle (Fig. 2). For example, the maximum $p_e(\theta)$ differences amongst the 13 predefined sampling schemes in the five plots ranged from 0.29 to 0.44 for zenith angle 0°, 0.07–0.16 for 30°, 0.03–0.09 for 57° and 0– 6.81×10^{-4} for 90°. Note that the $p_e(90)$ of all predefined sampling schemes in the five plots, except for plots 4 and 5, were equal to 0 (Fig. 2); $p_e(90)$ of all predefined sampling schemes, except for SS8–SS9, were equal to 0 in plot 4 (Fig. 2d); and

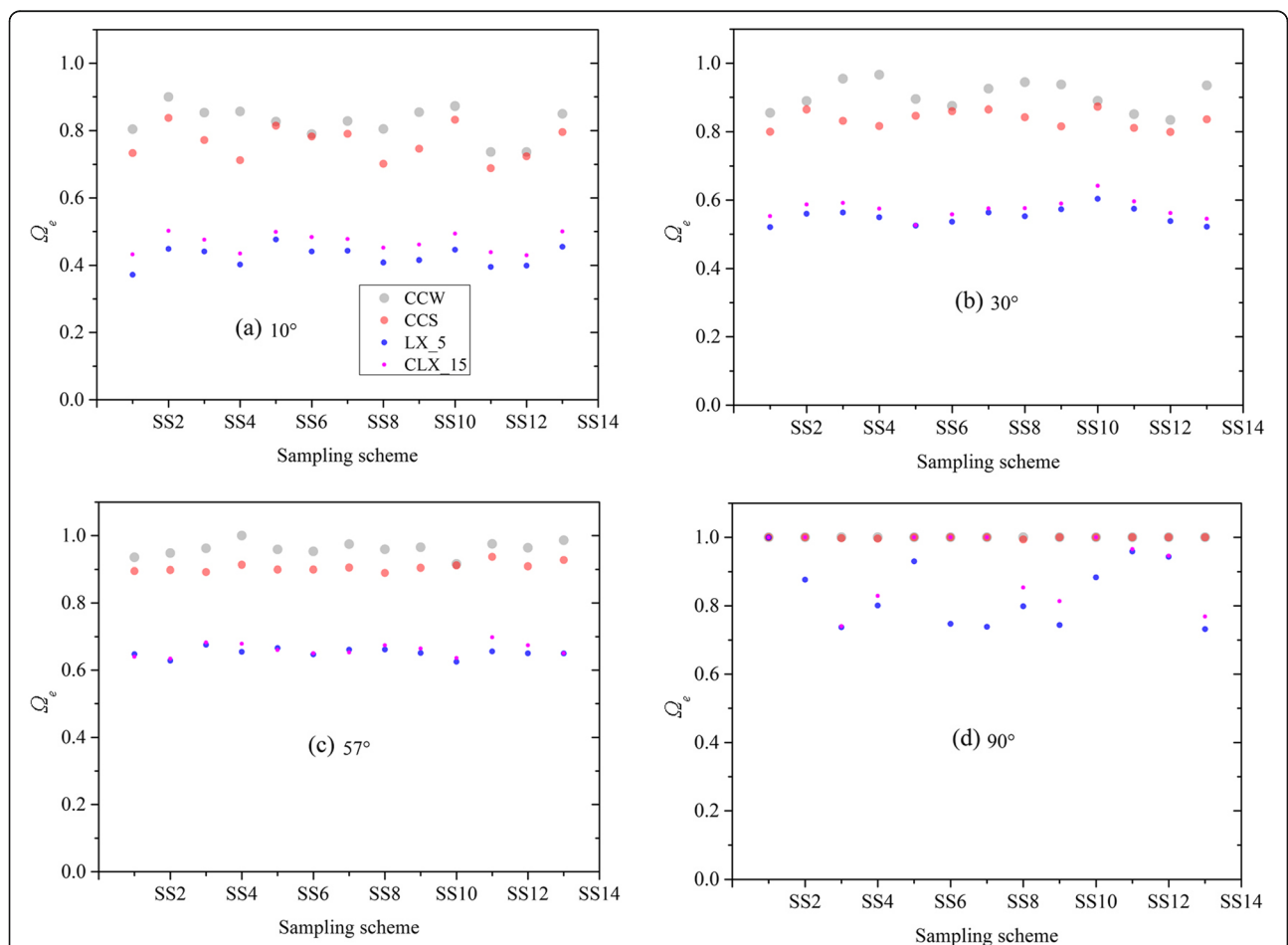
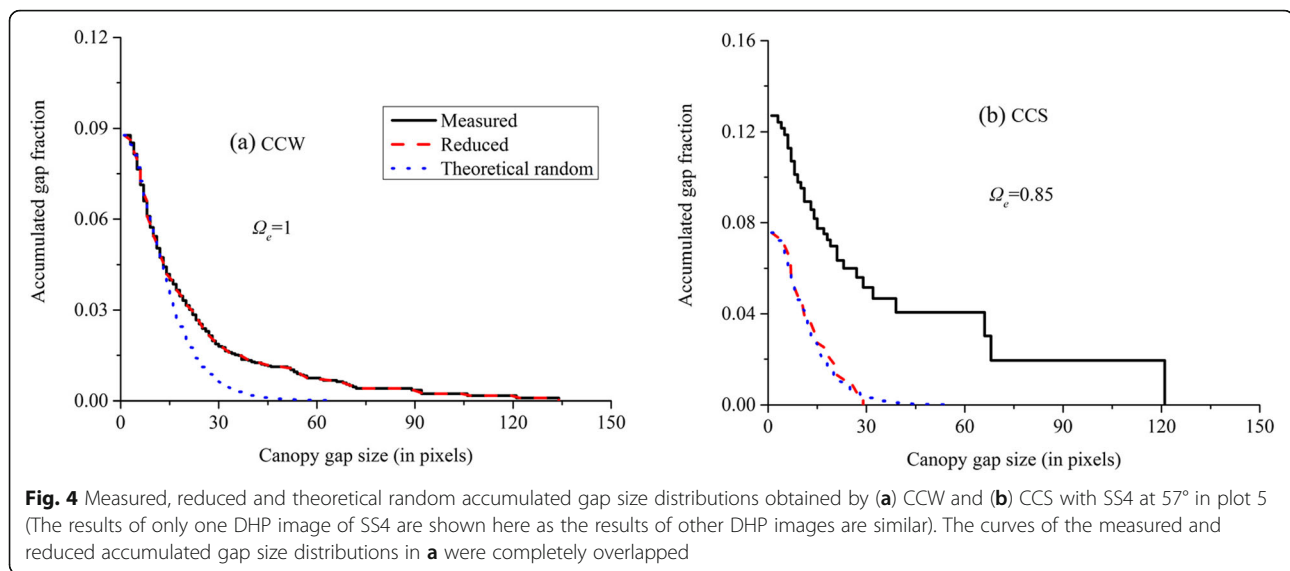


Fig. 3 Canopy element clumping indices (Ω_e) obtained using the four Ω_e algorithms (i.e. CCW, CCS, LX_5 and CLX_15) with the 13 predefined sampling schemes (SS1–SS13) at four zenith angles in plot 5 (a: 10°, b: 30°, c: 57° and d: 90°). Only plot 5 data are shown here as the other four plots showed similar behaviours



the $p_e(90)$ of all predefined sampling schemes ranged from 3.07×10^{-5} to 7.12×10^{-4} in plot 5 (Fig. 2e).

Effect of sampling schemes on canopy element clumping index (Ω_e) estimation

Similarly to the gap fraction, obvious variations were also found amongst the Ω_e from the 13 predefined sampling schemes, which were obtained using the same Ω_e algorithm at four typical zenith angles (i.e. 10°, 30°, 57° and 90°) in plot 5. The variations also seem to decrease with the zenith angle, except at 90° (Fig. 3). For example, the ranges of maximum variations amongst the Ω_e from the 13 predefined sampling schemes for the four Ω_e algorithms were 17%–28% (0.07–0.16) for the zenith angle of 0°, 9%–22% (0.07–0.13) for 30° and 5%–10% (0.05–0.08) for 57° (Fig. 3). Variations were also observed at 90°, especially for algorithms LX_5 and CLX_15. The ranges of variations amongst the Ω_e from the 13 predefined sampling schemes at 90° were 0%–0% (0–0), 0%–1% (0–0.01), 0%–37% (0–0.27) and 0%–35% (0–0.26) for CCW, CCS, LX_5 and CLX_15, respectively (Fig. 3d).

Figure 3 also shows that the Ω_e estimated with CCW was greater than that by CCS, which was obtained with the same scheme and zenith angle, for all predefined sampling schemes at the four zenith angles, except at 90°. In addition, the differences between the Ω_e from CCW and CCS under the same sampling scheme tended to increase with the increasing sample size at almost all zenith angles, except at 90°. For example, the differences between the Ω_e from CCW and CCS at 30° increased from 0.02 (3%) for SS2 to 0.12 (15%) for SS3 and 0.15 (18%) for SS4. An example of the gap removal procedure of the Ω_e estimation for CCW and CCS was presented (Fig. 4) to investigate the cause of the difference between Ω_e from CCW and CCS. For CCW, the gap fraction of

the largest gap size was small (8.62×10^{-4} for the gap size of 132 in pixels in the Fig. 4a example) because the length of the whole transect was large (153, 225 pixels) (Fig. 4a).

Effect of sampling schemes on PAI_e and LAI estimation

Obvious differences were observed amongst the PAI_e of the 13 predefined sampling schemes, which were estimated using the same inversion model in the five plots. The strength of the sampling scheme's impact on the PAI_e estimation varied with the inversion model (Fig. 5). The widest range of differences (0%–43%) amongst the PAI_e of the 13 predefined sampling schemes was found if Miller was used in the PAI_e estimation. By contrast, the range of differences amongst the PAI_e of the 13 predefined sampling schemes was narrowed to 0%–32% for Beer and 0%–30% for LAI-2200.

Fig. 6 shows that the LAI estimation was also largely affected by the sampling schemes. However, it is different from the PAI_e estimation since no large difference of the impact on LAI estimation was found amongst the three inversion models when the Ω_e algorithm of CCW was not used in the estimation. Specifically, the differences between the LAI obtained using the same inversion model and Ω_e algorithm amongst the four Ω_e algorithms, except CCW, under different predefined sampling schemes ranged from 0% to 36.2% (0–0.88) for Miller, 0%–35.1% (0–0.92) for LAI-2200 and 0%–37.6% (0–0.9) for Beer. When the Ω_e algorithm was CCW, the differences between the LAI obtained using the same inversion model under different predefined sampling schemes became larger, which ranged from 0% to 46.8% (0–0.79) for Miller, 0%–37.9% (0–0.69) for LAI-2200 and 0%–64.5% (0–0.75) for Beer.

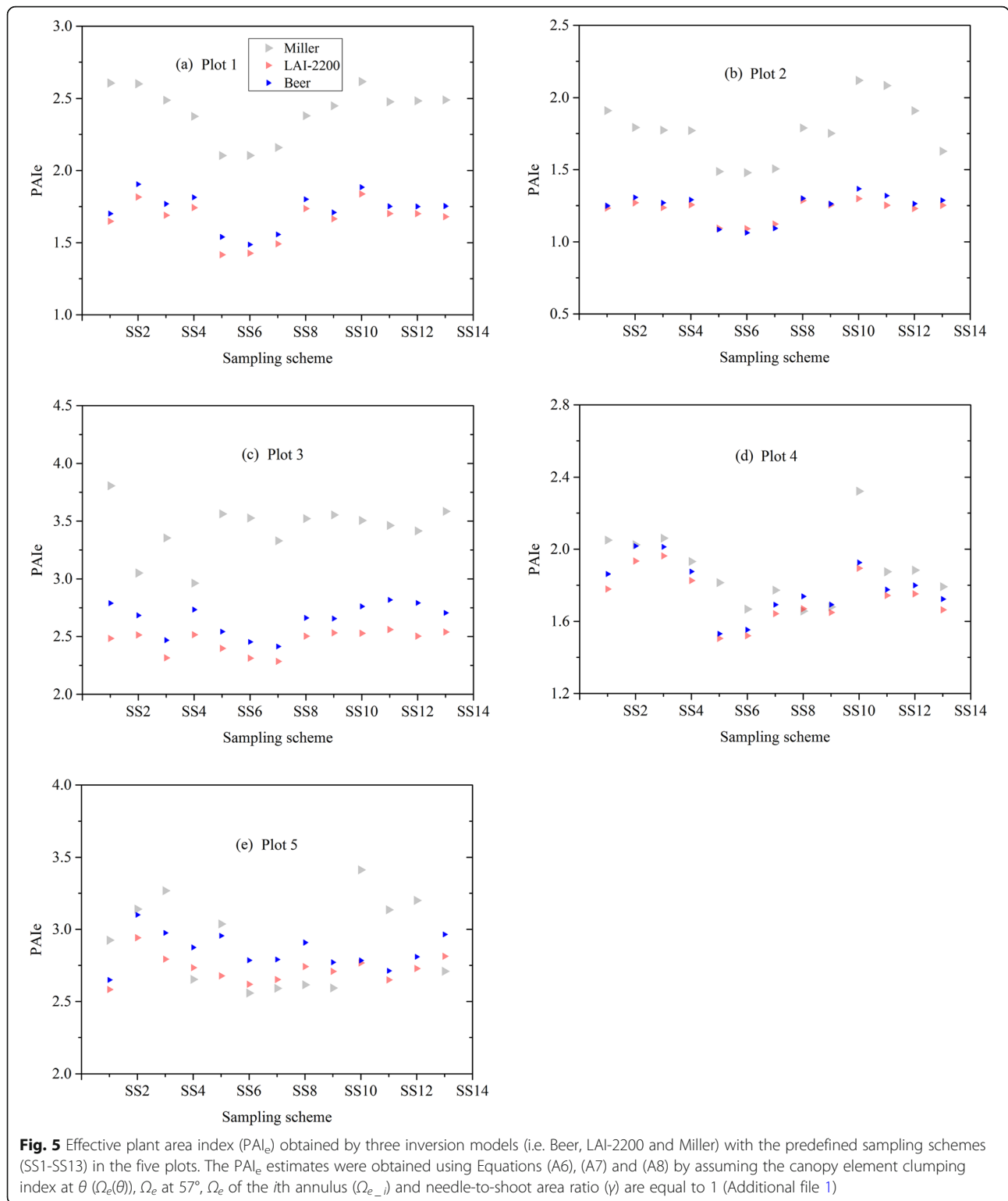


Fig. 6 also shows that all the LAI estimates obtained using the three inversion models and four Ω_e algorithms with 14 sampling schemes in the five plots were systematically smaller than the litter collection LAI. The underestimation

was especially obvious if CCW was adopted in the estimation, and it was reduced if CCW was replaced by CCS in the estimation (Fig. 6 and Table 2). For example, as shown in Table 2, the MREs of LAI obtained using Beer with 13

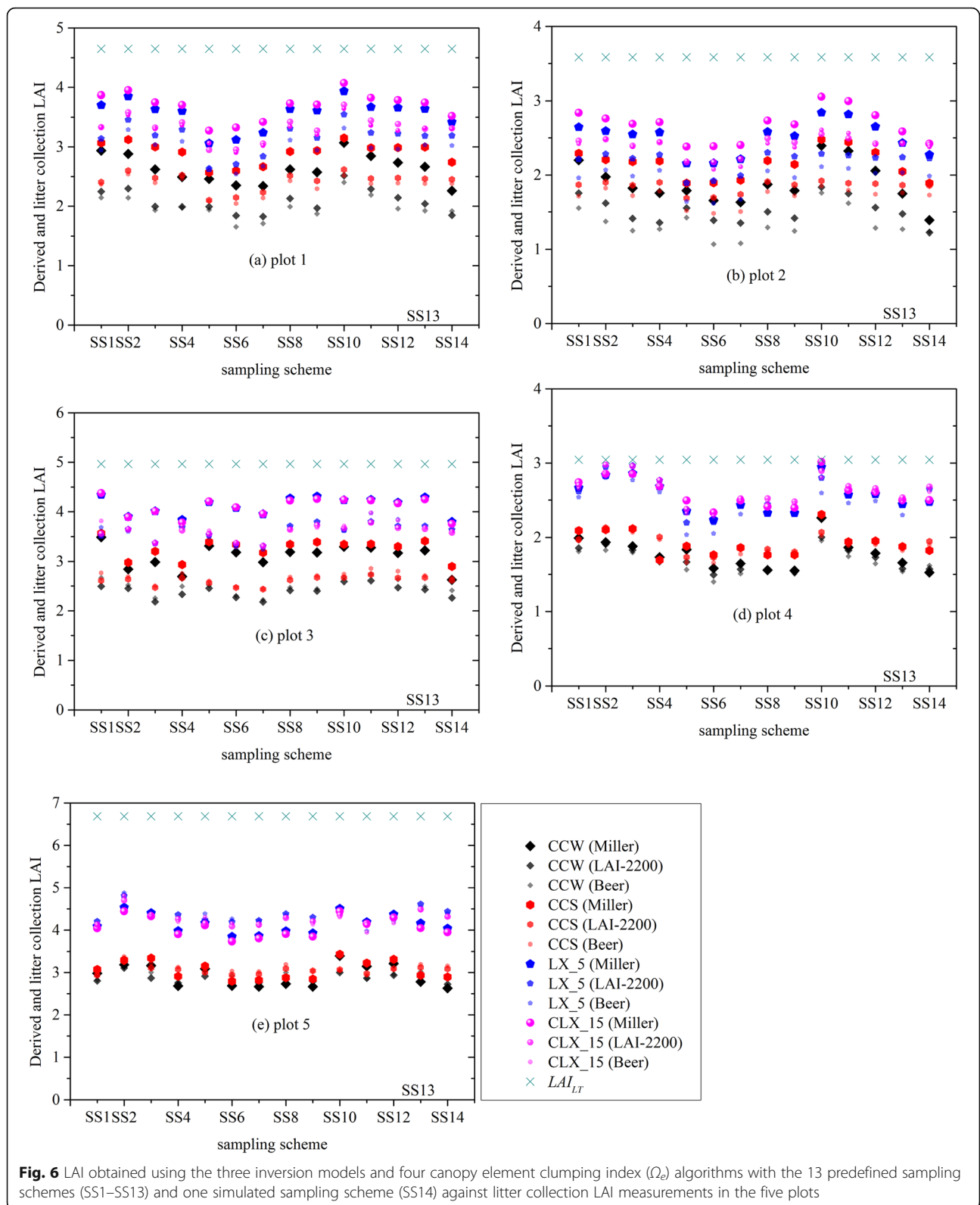


Fig. 6 LAI obtained using the three inversion models and four canopy element clumping index (Ω_e) algorithms with the 13 predefined sampling schemes (SS1–SS13) and one simulated sampling scheme (SS14) against litter collection LAI measurements in the five plots

Table 2 Mean relative errors (MREs) (%) of the LAI obtained with all the combinations of inversion model, canopy element clumping index (Ω_e) algorithm and sampling scheme. For each combination of inversion model and Ω_e algorithm, the four sampling schemes with the smallest MREs shown in red and the largest shown in green

| Inversion model | Miller | | | | LAI-2200 | | | | Beer | | | |
|-----------------|--------|------|------|--------|----------|------|------|--------|------|------|------|--------|
| | CCW | CCS | LX_5 | CLX_15 | CCW | CCS | LX_5 | CLX_15 | CCW | CCS | LX_5 | CLX_15 |
| SS1 | 39.0 | 36.7 | 22.0 | 19.7 | 49.9 | 47.0 | 30.2 | 27.4 | 51.0 | 47.5 | 32.6 | 27.0 |
| SS2 | 42.9 | 38.6 | 21.0 | 19.9 | 49.4 | 43.8 | 23.9 | 22.4 | 51.2 | 44.2 | 26.8 | 22.8 |
| SS3 | 44.7 | 38.1 | 22.0 | 21.0 | 54.1 | 45.7 | 27.6 | 26.3 | 54.8 | 46.8 | 31.0 | 27.0 |
| SS4 | 49.2 | 43.6 | 25.1 | 24.3 | 55.2 | 45.4 | 27.1 | 26.1 | 54.8 | 46.1 | 30.2 | 27.0 |
| SS5 | 44.8 | 42.9 | 30.0 | 27.0 | 53.2 | 50.8 | 36.8 | 32.8 | 53.9 | 51.6 | 38.9 | 31.9 |
| SS6 | 49.4 | 44.8 | 31.9 | 29.4 | 57.0 | 51.2 | 37.1 | 34.0 | 59.7 | 53.0 | 40.6 | 34.8 |
| SS7 | 50.0 | 44.3 | 30.2 | 28.1 | 57.3 | 49.9 | 34.7 | 32.2 | 59.3 | 51.8 | 38.3 | 33.3 |
| SS8 | 47.0 | 41.5 | 25.5 | 24.1 | 53.8 | 46.6 | 28.8 | 27.3 | 55.1 | 47.4 | 32.0 | 28.2 |
| SS9 | 47.9 | 41.6 | 25.9 | 24.6 | 55.6 | 47.4 | 30.0 | 28.4 | 56.9 | 49.0 | 33.6 | 29.6 |
| SS10 | 35.1 | 33.7 | 17.3 | 15.2 | 46.4 | 44.9 | 25.7 | 22.9 | 47.2 | 45.3 | 29.2 | 23.5 |
| SS11 | 39.9 | 37.6 | 21.9 | 20.0 | 49.3 | 46.3 | 28.5 | 26.0 | 50.5 | 47.0 | 31.4 | 26.1 |
| SS12 | 42.6 | 38.2 | 22.5 | 21.2 | 52.0 | 46.1 | 28.4 | 26.8 | 54.2 | 47.0 | 31.5 | 27.6 |
| SS13 | 46.6 | 40.8 | 24.9 | 23.8 | 54.1 | 46.7 | 28.8 | 27.4 | 55.4 | 47.5 | 32.1 | 27.7 |
| SS14 | 54.0 | 45.3 | 28.9 | 27.9 | 57.6 | 46.5 | 28.5 | 27.4 | 55.9 | 47.4 | 31.8 | 27.9 |

predefined sampling schemes ranged from 47.2% to 59.7% for CCW and reduced to 44.2%–53.0% for CCS. The smallest MRE was 15.2%, which was obtained using the combination of Miller, CLX_15 and SS10.

As shown in Table 2, the MREs of the LAI obtained using Miller and CLX_15 with the scheme with the largest sample size (SS14) was larger than those obtained using the same inversion model and Ω_e algorithm but with all predefined sampling schemes with smaller sample sizes (SS1–SS13), except for SS6 and SS7. The same tendency can be found

for the cases of two sampling scheme groups with the same sampling scheme type but with different sampling sizes, such as SS2–SS4 and SS10–SS11. For instance, the MREs of the LAI obtained using Miller and CLX_15 were 19.9% for SS2 with a sample size of 9, 21.0% for SS3 with a sample size of 16 and 24.3% for SS4 with a sample size of 25 (Table 2). Similarly, the MREs were 15.2% for SS10 with a sample size of 3 and increased to 20.0% for SS11 with a sample sizes of 5 if Miller and CLX_15 were adopted in the LAI estimation (Table 2).

Table 2 also shows that the performance of sampling schemes in the LAI estimation changes with the inversion models. For example, SS2 and SS10 outperformed the other 11 predefined sampling schemes in the LAI estimation if the inversion model was LAI-2200 or Beer due to the MREs of SS2 and SS10 were amongst the four smallest MREs of the LAI obtained using the same inversion model and Ω_e algorithm but with the 13 predefined sampling schemes (Table 2). Similarly, the MREs of SS10 and SS11 were amongst the four smallest MREs of the LAI obtained using the same inversion model and Ω_e algorithm with the 13 predefined sampling schemes if Miller was used in the estimation (Table 2). Note that most of the MREs of the LAI obtained with SS5, SS6, SS7 and SS9 were greater than those obtained using the same inversion model and Ω_e algorithm but with the other 9 predefined sampling schemes (Table 2).

Discussion

Are the Ω_e and LAI estimates markedly affected by sampling schemes?

Large differences were found amongst the Ω_e (0%–37%) obtained with the same Ω_e algorithm under different predefined sampling schemes (Figure 3) and amongst the LAI (0%–64.5%) estimated with the same inversion model and Ω_e algorithm under different sampling schemes in all the plots (Fig. 6). This finding indicates that both the Ω_e and LAI estimation are largely affected by the sampling scheme.

The large differences for Ω_e under different sampling schemes could be explained by the obvious differences for $p_e(\theta)$ under different sampling schemes (Fig. 2) given that all the Ω_e algorithms directly or indirectly relied on $p_e(\theta)$ to calculate Ω_e . The fact that the difference between Ω_e of CCW and CCS increases with the sample size for all the typical zenith angles, except at 90° , is primarily attributed to the incapability of CCW to effectively remove the large gaps (Fig. 4), which resulting from the nonrandom distribution of the canopy element in the gap removal procedure of the Ω_e estimation (Chen and Cihlar 1995b). This tendency indicated that the transect processing scheme is an important issue for CC in the Ω_e estimation. With the increase of transect length or sample size, the gap fraction of the same large gaps would be smaller. The variations between the LAIs obtained on the basis of the gap fraction estimates of the whole transect with or without the large gap sizes would tend to be smaller than the trigger condition of the gap removal procedure of CCW (< 0.01) (Chen and Cihlar 1995b). Larger Ω_e estimates would thus be obtained by CCW because large gaps were not effectively removed by the gap removal procedure in CCW (Fig. 4a). On the contrary, large gaps of the transects could be effectively distinguished and removed by CCS (Fig. 4b). Therefore,

the differences between the Ω_e of CCW and CCS increase with the sample size. Actually, many studies have also reported that CCW offers larger Ω_e estimates than other Ω_e algorithms, even though different PAI and plant function types of forest plots were covered in these studies (Pisek et al. 2011; Leblanc and Fournier 2014; Woodgate 2015; Zou et al. 2018a, 2018b). CCS could offer more accurate Ω_e than CCW due to the MREs of the LAI obtained using CCS were smaller than that using CCW under the condition of the same inversion model and sampling scheme (Table 2).

The obvious differences amongst the $p_e(\theta)$ or Ω_e from different sampling schemes would further result in large differences in PAI_e or LAI (Figs. 5 and 6, respectively) because $p_e(\theta)$ and Ω_e are the key parameters for PAI_e or LAI estimation (Equations A6–A8). The impact of the sampling schemes on PAI_e estimation was greater when the inversion model was Miller rather than the other two (i.e. LAI-2200 and Beer). An indication was that the variations of PAI_e obtained with different predefined sampling schemes ranged from 0% to 43% for Miller but only 0%–30% for LAI-2200 and 0%–32% for Beer (Fig. 5). One reason was identified in relation to the large range of variations for Miller. The $p_e(90)$ of all predefined sampling schemes in the five plots, except in plots 4 and 5, were equal to 0 (Fig. 2); the $p_e(90)$ of all predefined sampling schemes, except for SS8 and SS9, were equal to 0 in plot 4 (Fig. 2); and the $p_e(90)$ of all predefined sampling schemes ranged from 3.07×10^{-5} to 7.12×10^{-4} in plot 5 (Fig. 2). For Miller, the small variations between $p_e(\theta)$ measurements with zenith angles close to 90° , especially for those between zero and non-zero measurements, would result in obvious differences in PAI_e estimates. This outcome is attributed to the variations in $p_e(\theta)$ measurements being significantly enlarged by the logarithm of $p_e(\theta)$ in the PAI_e estimation (Equation A6) and the relatively large weight values ($\cos(\theta) \sin(\theta)$) at zenith angles close to 90° (not equal to 90°) compared to those at zenith angles close to zenith for Miller (Zou et al. 2018b). Compared with Miller, LAI-2200 or Beer can avoid the impact of zero or very small $p_e(\theta)$ measurements on the PAI_e estimation owing to the small zenith angle range covered by LAI-2200 (0° – 74°) or Beer (52° – 62°) and the large zenith angle width of the annulus of LAI-2200 (12° – 14°) or Beer (10°) (Zou et al. 2018b).

Different from PAI_e, the impact of sampling schemes on LAI estimation was not greater for Miller than the other two inversion models if CCW was not used in the estimation (Fig. 6 and Table 2). The reason could be attributed to the different zenith angle ranges covered by the three inversion models and the tendency of the variations amongst the $p_e(\theta)$ or Ω_e of different sampling schemes decreases with the zenith angle, except at 90° (Figs. 2 and 3).

Does increasing the sample size always improve LAI estimation accuracy?

The MREs of the LAI obtained with SS14, which has the largest sample size (i.e. 89), were not always smaller than those of the LAI obtained using the same inversion model and Ω_e algorithm but with all predefined sampling schemes with smaller sample sizes (i.e. from 3 to 25) (Table 2). The reason might be the overlap of canopy sampling of sample points in SS14 owing to the large sample size and relatively sparse spatial distribution of the sample points for SS14. The degree of overlap depends on the distance between the sample points and the canopy height, which is difficult to quantify because of the irregular spatial distribution of the sample points of SS14 in the heterogeneous forest plots. Furthermore, the MREs of the LAI obtained with SS4 were not the smallest amongst its sampling scheme group (i.e. SS2–SS4) to estimate LAI using the same inversion model and Ω_e algorithm, even though it had the largest sample size in the group. The same phenomenon was observed for the group of SS10 and SS11. Therefore, the accuracy of the LAI estimates obtained from DHP cannot always be improved with increasing sample sizes. Caution is needed if the LAI estimates obtained with the sampling schemes having large sample sizes are treated as the estimates with high accuracy or even as reference estimates. Previous studies (e.g. Nackaerts et al. 2000; Majasalmi et al. 2012; Calders et al. 2018) treated the PAI_e or effective woody area index estimates from sampling schemes with large sample sizes as highly accurate results or even as reference for validation which should provide more specific analyses.

Which sampling scheme(s) is (are) more reliable to estimate the LAI of forest plots?

The best sampling schemes for estimating the ESU LAI of *L. principis-rupprechtii* forests varied with the different inversion models used (Table 2). The two sampling scheme groups of SS2, SS10 and SS10, SS11 are recommended for use to estimate the ESU LAI of *L. principis-rupprechtii* forests if LAI-2200 or Beer and Miller were adopted in the estimation. A common characteristic of SS2, SS10 and SS11 is their small sample sizes (i.e. 3–9). This means that an accurate estimation of the ESU LAI of *L. principis-rupprechtii* forest plots does not need sampling schemes with large sample sizes, which are very cost-effective for the long time series field measurements of forest ESU LAI to validate LAI products.

Amongst the 13 predefined sampling schemes, SS5–SS7 and SS9 are not recommended for use owing to their relatively large MREs compared with the MREs of the LAI obtained using the same inversion model and Ω_e algorithm, except for CCW, but with the other nine predefined sampling schemes (Table 2).

SS6 and SS7 are likewise not recommendable because they have the largest MREs in their own sampling scheme groups (with the same or similar sample sizes but with different sampling scheme types). Specifically, SS6 belongs to the group that made up SS2, SS6 and SS12 with a sample size of 9, whilst SS7 belongs to the group of SS7, SS8 and SS13 with the same or similar sample sizes ranging from 12 to 13. The large MREs for SS5–SS7 may be caused by an undersampling or oversampling of the four corners or centre areas of the plots because the sampling points of those sampling schemes are distributed along or near the two perpendicular centre lines of the plots. The poor performance of SS5–SS7 in this study is inconsistent with the conclusions of Majasalmi et al. (2012), who concluded that cross sampling schemes similar to SS5–SS7 in this study outperformed other sampling schemes in the PAI_e estimation of forest plots. Three reasons can be responsible for the conflicting conclusions from the two studies. First, only the impact of sampling schemes on the PAI_e was investigated in Majasalmi et al. (2012), which should be different from that on LAI given that Ω_e is additionally required for LAI estimation. Furthermore, Ω_e was largely affected by the sampling schemes (Fig. 3). Second, different references were used to evaluate the accuracy of retrievals from different sampling schemes in the two studies. The PAI_e estimates of sampling scheme with the largest sample size were used as reference in Majasalmi et al. (2012), whereas litter collection LAI measurements were used in the current study. However, the results of this study showed that LAI obtained from the sampling scheme with the largest sample size (SS14) is not the one with the highest accuracy (Fig. 6 and Table 2). Third, the sampling schemes used in the two studies are not completely the same, especially for the square and dispersed sampling schemes.

Can accurate ESU LAI with estimation errors below 5% or 20% be obtained from DHP using the 13 predefined sampling schemes?

LAI underestimation was observed for all the combinations of inversion model, Ω_e algorithm and sampling scheme in the five plots (Fig. 6). This finding can be attributed to two reasons. First, previous studies reported that optical methods tend to underestimate the LAI of forest plots when the LAI (not PAI) is large, especially for a closed canopy with an LAI larger than approximately 5 or 6, due to the gap fraction saturation issue for optical methods (Gower et al. 1999; Jonckheere et al. 2004). Evident LAI underestimation of optical methods in coniferous forest plots with large LAI values was also reported by Chen et al. (1997). They presented a large

difference of 45% between the LAI of optical methods and the allometric measurements in an old black spruce plot with an LAI of 6.3. As one of the optical methods, DHP underestimated LAI in plot 5 with an LAI of 6.69 obviously in this study (Fig. 6). Second, most shoots whose petioles measure about 1–4 mm are located directly on the surfaces of the branches and stems of *L. principis-rupprechtii* forest plots. Therefore, the overlap of shoots and woody components will make DHP unable to sample canopies sufficiently, leading to Ω_e overestimation and further LAI underestimation. Moreover, because branches in the bottom level of plots 1 and 2 were harvested by management activities, most shoots that were detected by DHP sensor were located in the middle and upper level of the canopies. Long-distance detection reduces the effectiveness of canopy sampling and therefore, results in LAI underestimation.

Amongst all the combinations of inversion model, Ω_e algorithm and sampling scheme, the LAI with the two smallest MREs (i.e. 10.7% and 13.5%) were obtained using the combinations of Miller and SS10 with the two Ω_e algorithms of CLX_15 and LX_5, respectively (Table 2). The two MREs of our study are close to those of Leblanc and Fournier (2014), who reported a minimum MRE of 11% for the PAI obtained from DHP if the appropriate inversion model and Ω_e algorithm were adopted in the PAI estimation of the simulated forest scenes. It was expected that one of the two MREs of this study would be slightly larger than those of the simulation study. Two reasons were identified in relation to the relatively large MRE of this study. First, compared with the simulation study, the field LAI measurements of DHP usually include two more LAI estimation error sources (i.e. observation conditions and DHP image classification). Second, the estimates obtained from the simulation study are PAI, not the LAI of this study. The conversion from PAI into LAI would introduce additional estimation errors from the α measurements.

Table 2 shows that the ESU LAI estimates obtained by our study did not match the maximum LAI estimation error threshold of 5% set by GCOS. The reason for this is that the MREs of the LAI obtained using all the combinations of inversion model, Ω_e algorithm and sampling scheme are larger than 5% (Table 2). The LAI differences between litter collection LAI measurements and those obtained by DHP with all the possible combinations of inversion models, Ω_e algorithms and sampling schemes are also larger than 5% in the five *L. principis-rupprechtii* plots, except in plot 4 (Fig. 6). However, ESU LAI estimates with the MREs below 20% could be obtained if appropriate combinations of inversion model, Ω_e algorithm and sampling scheme were adopted in the LAI estimation of *L. principis-rupprechtii* forest plots (Table 2). Specifically, ESU LAI estimates with relatively

small MREs (ranging from 10.7% to 20.0%) can be obtained for all plots, except plot 5, using Miller and CLX_15 with SS1–SS13, with the exception of the four sampling schemes of SS5–SS7 and SS9. The LAI differences between litter collection LAI measurements and those obtained from DHP using Miller and CLX_15 with SS10 or SS11 are lower than 20% in the five plots, except plot 5 (Fig. 6). This result indicates that ESU LAI estimates with the maximum LAI estimation errors below 20%, which is required by GCOS, can be obtained from DHP if the appropriate inversion model, Ω_e algorithm and sampling scheme were adopted. This conclusion is at least effective for *L. principis-rupprechtii* forest plots, except for those with extremely large LAI values (e.g. 6.69 for plot 5), because wide canopy structure characteristics were covered by the five plots in this study (Table 1).

Conclusions

The impact of sampling schemes on the ESU LAI estimation from DHP in the five *L. principis-rupprechtii* forests was evaluated in this study. Results showed obvious differences amongst the $p_e(\theta)$, Ω_e , PAI_e and LAI from different sampling schemes. The differences in impact of the sampling schemes on LAI estimation were not obvious amongst the three inversion models (i.e. Miller, LAI-2200 and Beer) if the Ω_e algorithm of CCW was not adopted in the estimation. The accuracy of the ESU LAI estimates was not always improved by increasing the sample sizes. The two sampling scheme groups of SS2, SS10 and SS10, SS11 (with sample sizes ranging from 3 to 9) outperformed other predefined sampling schemes to obtain the ESU LAI of *L. principis-rupprechtii* forests if Beer or LAI-2200 and Miller were adopted in the estimation, respectively. SS5–SS7 and SS9 are not recommended for use owing to their relatively large MREs. Moreover, ESU LAI estimates with maximum LAI estimation errors below 20%, which is required by GCOS, could be achieved by DHP if the appropriate inversion model, Ω_e algorithm and sampling scheme were adopted in the LAI estimation of *L. principis-rupprechtii* forests, except for those with extremely large LAI values. However, DHP is still not qualified for obtaining ESU LAI estimates of *L. principis-rupprechtii* forests with maximum LAI estimation errors below 5%, regardless of which combination of inversion model, Ω_e algorithm and sampling scheme is adopted in the estimation.

Future work can include efforts to investigate the impact of sampling schemes on the ESU LAI estimation of forests from other indirect LAI measurement methods (e.g. terrestrial laser scanner and LAI-2200). Since the differences between the canopy structures of different plant functional types, caution is needed if the conclusion of this study is applied to forests with tree species other than the *L. principis-rupprechtii* covered in this

study. Therefore, forest plots with different plant functional types can also be included to consolidate the conclusions of this study. Furthermore, the complicated issue of canopy sampling overlap between different sample points is worth analysing in the future.

Nomenclature

A_n : half of the total needle area in a shoot;

$A_p(0^\circ, 0^\circ)$: projection area of shoot sample measured by projecting the shoot at zenith angle 0° and azimuth angle 0° ;

$A_p(45^\circ, 0^\circ)$: projection area of shoot sample measured by projecting the shoot at zenith angle 45° and azimuth angle 0° ;

$A_p(90^\circ, 0^\circ)$: projection area of shoot sample measured by projecting the shoot at zenith angle 90° and azimuth angle 0° ;

Beer: Beer inversion model (Equation A7);

CC: gap-size analysis algorithm;

CLX: combination of gap-size and finite-length averaging algorithms;

CLX_15: combination of gap-size and finite-length averaging algorithms with a segment size of 15° ;

CCS: gap-size analysis algorithm for deriving Ω_e of forest canopies by averaging the Ω_e of all DHP images of sampling schemes;

CCW: gap-size analysis algorithm for estimating the Ω_e of forest canopies based on the gap size distributions merged from the gap size distributions of all DHP images of sampling schemes;

DBH: diameter at breast height;

DHP: Digital Hemispherical Photography;

$F_m(0, \theta)$: measured total canopy element gap fraction at θ ;

$F_{mr}(0, \theta)$: total canopy element gap fraction after removing the large gaps resulting from the nonrandom distribution of the canopy element at θ ;

GCOS: Global Climate Observing System;

G_e : canopy element projection coefficient;

$G_e(\theta)$: canopy element projection coefficient at θ ;

G_{e_i} : canopy element projection coefficient of the i th annulus;

LAI: leaf area index;

LAI-2200: LAI-2200 inversion model (Equation A8);

$\ln[\bar{p}_e(\theta)]$: mean logarithmic canopy element gap fraction for all segments at θ ;

LX: finite-length averaging algorithm;

LX_5: finite-length averaging algorithm with a segment size of 5° ;

MRE: mean relative error;

Miller: Miller theorem (Equation A6);

$p_e(\theta)$: canopy element gap fraction at θ ;

$\bar{p}_e(\theta)$: mean canopy element gap fraction of all segments at θ ;

p_{e_i} : canopy element gap fraction of the i th annulus;

$p_{e_k}(\theta)$: canopy element gap fraction of segment k at θ ;

PAI_e: effective plant area index;

PAI: plant area index;

PAI_{Beer}: plant area index estimated based on the Beer inversion model;

PAI_{LAI-2200}: plant area index estimated based on the modified Miller theorem of LAI-2200 instrument;

PAI_{Miller}: plant area index estimated based on the Miller theorem;

W_i : weight of the i th annulus of DHP images in the Leaf Area Index or Plant Area Index estimation;

θ : zenith angle;

θ_i : centre zenith angle of the i th annulus;

α : woody-to-total area ratio;

γ_e : effective needle-to-shoot area ratio;

γ : needle-to-shoot area ratio;

n : number of segments;

Ω_e : canopy element clumping index;

$\Omega_e(\theta)$: canopy element clumping index at θ ;

$\Omega_{e_CC}(\theta)$: canopy element clumping index estimated using the gap-size analysis algorithm at θ ;

$\Omega_{e_CC_k}(\theta)$: Ω_e of segment k at θ estimated using CC;

$\Omega_{e_LX}(\theta)$: canopy element clumping index estimated using the finite-length averaging algorithm at θ ;

$\Omega_{e_CLX}(\theta)$: canopy element clumping index estimated using the combination of gap-size and finite-length averaging algorithm at θ ;

$\Omega_{e_i}(\theta)$: Ω_e of the i th annulus calculated by averaging $\Omega_e(\theta)$ with the zenith angles covered by the i th annulus.

Supplementary information

Supplementary information accompanies this paper at <https://doi.org/10.1186/s40663-020-00262-z>.

Additional file 1. PAI estimation.

Acknowledgements

Funding for this work came from the National Science Foundation of China (Grant Nos. 41871233, 41371330 and 41001203).

Authors' contributions

Jie Zou participated in study design, field measurements, data processing, interpreting the results and writing the manuscript. Peng Leng took part in the field measurements. Wei Hou, Yong Zuo and Peihong Zhong took part in the procedure of data processing. Ling Chen, Qianfeng Wang and Shezhou Luo participated in the writing of the paper. The author(s) read and approved the final paper.

Availability of data and materials

The datasets used and/or analysed during the current study are available from the corresponding author on reasonable requests.

Ethics approval and consent to participate

Not applicable.

Consent for publication

Not applicable.

Competing interests

The authors declare that they have no competing interests.

Author details

¹The Academy of Digital China (Fujian), Fuzhou University, Fuzhou 350116, China. ²Key Laboratory of Data Mining and Information Sharing, Ministry of Education, Fuzhou 350116, China. ³School of Forestry, Beijing Forestry University, Beijing 100083, China. ⁴College of Environment and Resources, Fuzhou University, Fuzhou 350116, China. ⁵College of Resources and Environment, Fujian Agriculture and Forestry University, Fuzhou 350002, China.

Received: 9 April 2020 Accepted: 21 July 2020

Published online: 24 August 2020

References

- Abuelgasim AA, Fernandes RA, Leblanc SG (2006) Evaluation of national and global LAI products derived from optical remote sensing instruments over Canada. *IEEE Trans Geosci Remote Sens* 44:1872–1884. <https://doi.org/10.1109/TGRS.2006.874794>
- Baret F, Weiss M, Allard D, Garrigue S, Leroy M, Jeanjean H, Fernandes R, Myneni R, Privette J, Morisette J, Bohbot H, Bosseno R, Dedieu G, Bella C, Duchemin B, Espana M, Gond V, Gu X, Guyon D, Lelong C, Maisongrande P, Mougouin E, Nilson T, Veroustraete F, Vintilla R (2005) VALERI: a network of sites and a methodology for the validation of medium spatial resolution satellite products. <http://w3.avignon.inra.fr/valeri/documents/VALERI-RSESubmitted.pdf>. Accessed 18 Oct 2019
- Calders K, Origo N, Disney M, Nightingale J, Woodgate W, Armston J, Lewis P (2018) Variability and bias in active and passive ground-based measurements of effective plant, wood and leaf area index. *Agric Forest Meteorol* 252:231–240. <https://doi.org/10.1016/j.agrformet.2018.01.029>
- Cao B, Du YM, Li J, Li H, Li L, Zhang Y, Zou J, Liu QH (2015) Comparison of five slope correction methods for leaf area index estimation from hemispherical photography geoscience and remote sensing letters. *IEEE* 12:1958–1962. <https://doi.org/10.1109/LGRS.2015.2440438>
- Chen J (2014) Remote sensing of leaf area index of vegetation covers. In: Weng Q (ed) *Remote sensing of natural resources*. CRC Press, USA
- Chen JM, Black TA (1992) Defining leaf area index for non-flat leaves. *Plant Cell Environ* 15:421–429. <https://doi.org/10.1111/j.1365-3040.1992.tb00992.x>
- Chen JM, Cihlar J (1995a) Plant canopy gap-size analysis theory for improving optical measurements of leaf-area index. *Appl Opt* 34:6211–6222. <https://doi.org/10.1364/AO.34.006211>
- Chen JM, Cihlar J (1995b) Quantifying the effect of canopy architecture on optical measurements of leaf area index using two gap size analysis methods. *IEEE Trans Geosci Remote Sens* 33:777–787. <https://doi.org/10.1109/36.387593>
- Chen JM, Govind A, Sonnentag O, Zhang Y, Barr A, Amiro B (2006) Leaf area index measurements at Fluxnet-Canada forest sites. *Agric Forest Meteorol* 140:257–268. <https://doi.org/10.1016/j.agrformet.2006.08.005>
- Chen JM, Rich PM, Gower ST, Norman JM, Plummer S (1997) Leaf area index of boreal forests: theory, techniques and measurements. *J Geophys Res* 102: 29429–29443. <https://doi.org/10.1029/97JD01107>
- Cutini A, Matteucci G, Mugnozza GS (1998) Estimation of leaf area index with the Li-Cor LAI 2000 in deciduous forests. *Forest Ecol Manag* 105:55–65. [https://doi.org/10.1016/S0378-1127\(97\)00269-7](https://doi.org/10.1016/S0378-1127(97)00269-7)
- Ercanlı I, Günlü A, Şenyurt M, Keleş S (2018) Artificial neural network models predicting the leaf area index: a case study in pure even-aged Crimean pine forests from Turkey. *For Ecosyst* 5:29. <https://doi.org/10.1186/s40663-018-0149-8>
- Fang H, Jiang C, Li W, Wei S, Baret F, Chen JM, Garcia-Haro J, Liang S, Liu R, Myneni RB, Pinty B, Xiao Z, Zhu Z (2013) Characterization and intercomparison of global moderate resolution leaf area index (LAI) products: analysis of climatologies and theoretical uncertainties. *J Geophys Res Biogeosci* 118:529–548. <https://doi.org/10.1002/jgrg.20051>
- Fernandes R, Plummer S, Nightingale J, Baret F, Camacho F, Fang H, Garrigues S, Gobron N, Lang M, Lacaze R, LeBlanc S, Meroni M, Martinez B, Nilson T, Pinty B, Pisek J, Sonnentag O, Verger A, Welles J, Weiss M, Widlowski JL (2014) Global leaf area index product validation good practices (version 2.0). Land Product validation subgroup (WGCV/CEOS), Roma, Italy. doi:<https://doi.org/10.5067/doc/ceoswgcv/lpv/lai.002>
- Garrigues S, Lacaze R, Baret F, Morisette JT, Weiss M, Nickeson JE, Fernandes R, Plummer S, Shabanov NV, Myneni RB, Knyazikhin Y, Yang W (2008) Validation and intercomparison of global leaf area index products derived from remote sensing data. *J Geophys Res Biogeosci* 113. <https://doi.org/10.1029/2007JG000635>
- Gonsamo A, Pellikka P (2008) Methodology comparison for slope correction in canopy leaf area index estimation using hemispherical photography. *For Ecol Manag* 256:749–759. <https://doi.org/10.1016/j.foreco.2008.05.032>
- Gonsamo A, Pellikka P (2009) The computation of foliage clumping index using hemispherical photography. *Agric Forest Meteorol* 149:1781–1787. <https://doi.org/10.1016/j.agrformet.2009.06.001>
- Gonsamo A, Walter J-MN, Pellikka P (2010) Sampling gap fraction and size for estimating leaf area and clumping indices from hemispherical photographs. *Can J For Res* 40:1588–1603. <https://doi.org/10.1139/X10-085>
- Gower ST, Kucharik CJ, Norman JM (1999) Direct and indirect estimation of leaf area index, fAPAR, and net primary production of terrestrial ecosystems. *Remote Sens Environm* 70:29–51. [https://doi.org/10.1016/S0034-4257\(99\)00056-5](https://doi.org/10.1016/S0034-4257(99)00056-5)
- Hyer EJ, Goetz SJ (2004) Comparison and sensitivity analysis of instruments and radiometric methods for LAI estimation: assessments from a boreal forest site. *Agric Forest Meteorol* 122:157–174. <https://doi.org/10.1016/j.agrformet.2003.09.013>
- Jonckheere I, Fleck S, Nackaerts K, Muys B, Coppin P, Weiss M, Baret F (2004) Review of methods for in situ leaf area index determination: part I. theories, sensors and hemispherical photography. *Agric Forest Meteorol* 121:19–35. <https://doi.org/10.1016/j.agrformet.2003.08.027>
- Kucharik CJ, Norman JM, Murdock LM, Gower ST (1997) Characterizing canopy nonrandomness with a multiband vegetation imager (MVI). *J Geophys Res Atm* 102:29455–29473. <https://doi.org/10.1029/97JD01175>
- Lang ARG, Yueqin X (1986) Estimation of leaf area index from transmission of direct sunlight in discontinuous canopies. *Agric Forest Meteorol* 37:229–243. [https://doi.org/10.1016/0168-1923\(86\)90033-X](https://doi.org/10.1016/0168-1923(86)90033-X)
- Leblanc SG (2008) DHP-TRACWin MANUAL. CCRS technical Repor. ftp://ftp.ccrs.nrcan.gc.ca/ad/LEBLANC/SOFTWARE/DHP/DHP-TRACWIN_MANUAL.pdf. Accessed 18 Oct 2019
- Leblanc SG, Chen JM (2001) A practical scheme for correcting multiple scattering effects on optical LAI measurements. *Agric Forest Meteorol* 110:125–139. [https://doi.org/10.1016/S0168-1923\(01\)00284-2](https://doi.org/10.1016/S0168-1923(01)00284-2)
- Leblanc SG, Chen JM (2002) Tracing radiation and architecture of canopies TRAC manual version 2.1.3. Natural Resources Canada, Ottawa, Ontario, Canada
- Leblanc SG, Chen JM, Fernandes R, Deering DW, Conley A (2005) Methodology comparison for canopy structure parameters extraction from digital hemispherical photography in boreal forests. *Agric Forest Meteorol* 129:187–207. <https://doi.org/10.1016/j.agrformet.2004.09.006>
- Leblanc SG, Fournier RA (2014) Hemispherical photography simulations with an architectural model to assess retrieval of leaf area index. *Agric Forest Meteorol* 194:64–76. <https://doi.org/10.1016/j.agrformet.2014.03.016>
- Li-COR (2009) LAI-2200 plant canopy analyzer instruction manual. Li-Cor Cor, Lincoln
- Liu Z, Jin G, Chen J, Qi Y (2015) Evaluating optical measurements of leaf area index against litter collection in a mixed broadleaved-Korean pine forest in China. *Trees* 29:59–73. <https://doi.org/10.1007/s00468-014-1058-2>
- Macfarlane C, Hoffman M, Eamus D, Kerp N, Higginson S, McMurtrie R, Adams M (2007) Estimation of leaf area index in eucalypt forest using digital photography. *Agric Forest Meteorol* 143:176–188. <https://doi.org/10.1016/j.agrformet.2006.10.013>
- Majasalmi T, Rautiainen M, Stenberg P, Rita H (2012) Optimizing the sampling scheme for LAI-2000 measurements in a boreal forest. *Agric Forest Meteorol* 154–155:38–43. <https://doi.org/10.1016/j.agrformet.2011.10.002>
- Miller J (1967) A formula for average foliage density. *Aust J Bot* 15:141–144. <https://doi.org/10.1071/BT9670141>
- Nackaerts K, Coppin P, Muys B, Hermy M (2000) Sampling methodology for LAI measurements with LAI-2000 in small forest stands. *Agric Forest Meteorol* 101(4):247–250. [https://doi.org/10.1016/S0168-1923\(00\)00090-3](https://doi.org/10.1016/S0168-1923(00)00090-3)
- Neumann HH, Den Hartog G, Shaw RH (1989) Leaf area measurements based on hemispheric photographs and leaf-litter collection in a deciduous forest during autumn leaf-fall. *Agric Forest Meteorol* 45:325–345. [https://doi.org/10.1016/0168-1923\(89\)90052-X](https://doi.org/10.1016/0168-1923(89)90052-X)
- Nilson T (1999) Inversion of gap frequency data in forest stands. *Agric Forest Meteorol* 98–99:437–448. [https://doi.org/10.1016/S0168-1923\(99\)00114-8](https://doi.org/10.1016/S0168-1923(99)00114-8)
- Pfeifer M, Gonsamo A, Woodgate W, Cayuela L, Marshall AR, Ledo A, Paine TCE, Marchant R, Burt A, Calders K, Courtney-Mustaphi C, Cuni-Sanchez A, Deere NJ, Denu D, de Tanago JG, Hayward R, Lau A, Macía MJ, Olivier PI, Pellikka P, Seki H, Shirima D, Trevithick R, Wedeux B, Wheeler C, Munishi PKT, Martin T, Mustari A,

- Platts PJ (2018) Tropical forest canopies and their relationships with climate and disturbance: results from a global dataset of consistent field-based measurements. For Ecosyst 57. <https://doi.org/10.1186/s40663-017-0118-7>
- Pisek J, Lang M, Nilson T, Korhonen L, Karu H (2011) Comparison of methods for measuring gap size distribution and canopy nonrandomness at Järvselja RAMI (RAAdiation transfer model Intercomparison) test sites. Agric Forest Meteorol 151:365–377. <https://doi.org/10.1016/j.agrformet.2010.11.009>
- Ross J (1981) The radiation regime and architecture of plant stands. Dr. W. Junk Publishers, The Hague
- Running SW, Hunt ER (1993) Generalization of a forest ecosystem process model for other biomes, BIOME-BGC, and an application for global-scale models. In: Ehleringer JR, Field C (eds) Scaling physiological processes: leaf to globe. Academic Press, San Diego, pp 141–158
- Ryu Y, Nilson T, Kobayashi H, Sonnentag O, Law BE, Baldocchi DD (2010b) On the correct estimation of effective leaf area index: does it reveal information on clumping effects? Agric Forest Meteorol 150:463–472. <https://doi.org/10.1016/j.agrformet.2010.01.009>
- Ryu Y, Sonnentag O, Nilson T, Vargas R, Kobayashi H, Wenk R, Baldocchi DD (2010a) How to quantify tree leaf area index in an open savanna ecosystem: a multi-instrument and multi-model approach. Agric Forest Meteorol 150:63–76. <https://doi.org/10.1016/j.agrformet.2009.08.007>
- Soto-Berelov M, Jones S, Farmer E, Woodgate E (2015) Review of validation standards of biophysical earth observation products. In: Held A, Phinn S, Soto-Berelov M, Jones S (eds) AusCover Good Practice Guidelines: A technical handbook supporting calibration and validation activities of remotely sensed data product. TERN AusCover, pp 8–32
- van Gardingen PR, Jackson GE, Hernandez-Daumas S, Russell G, Sharp L (1999) Leaf area index estimates obtained for clumped canopies using hemispherical photography. Agric Forest Meteorol 94:243–257. [https://doi.org/10.1016/S0168-1923\(99\)00018-0](https://doi.org/10.1016/S0168-1923(99)00018-0)
- Walter J-MN, Fournier RA, Soudani K, Meyer E (2003) Integrating clumping effects in forest canopy structure: an assessment through hemispherical photographs. Can J Remote Sens 29:388–410. <https://doi.org/10.5589/m03-011>
- Watson DJ (1947) Comparative physiological studies in the growth of field crops. I. Variation in net assimilation rate and leaf area between species and varieties, and within and between years. Ann Bot 11:41–76. <https://doi.org/10.1093/oxfordjournals.aob.a083148>
- Weiss M, Baret F, Smith GJ, Jonckheere I, Coppin P (2004) Review of methods for in situ leaf area index (LAI) determination: part II. Estimation of LAI, errors and sampling. Agric Forest Meteorol 121:37–53. <https://doi.org/10.1016/j.agrformet.2003.08.001>
- Woodgate W (2015) In-situ leaf area index estimate uncertainty in forests: supporting earth observation product calibration and validation. PhD Thesis. RMIT University, Melbourne
- Woodgate W, Jones SD, Suarez L, Hill MJ, Armston JD, Wilkes P, Soto-Berelov M, Haywood A, Mellor A (2015) Understanding the variability in ground-based methods for retrieving canopy openness, gap fraction, and leaf area index in diverse forest systems. Agric Forest Meteorol 205:83–95. <https://doi.org/10.1016/j.agrformet.2015.02.012>
- Woodgate W, Soto-Berelov M, Suarez L, Jones S, Hill M, Wilkes P, Axelsson C, Haywood A, Mellor A (2012) Searching for the optimal sampling design for measuring LAI in an upland rainforest. Proceedings of the 2012 Geospatial science research 3 symposium (GSR_2), Melbourne, Australia
- Yan G, Hu R, Luo J, Weiss M, Jiang H, Mu X, Xie D, Zhang W (2019) Review of indirect optical measurements of leaf area index: recent advances, challenges, and perspectives. Agric Forest Meteorol 265:390–411. <https://doi.org/10.1016/j.agrformet.2018.11.033>
- Zhang Y, Chen JM, Miller JR (2005) Determining digital hemispherical photograph exposure for leaf area index estimation. Agri Forest Meteorol 133:166–181. <https://doi.org/10.1016/j.agrformet.2005.09.009>
- Zou J, Leng P, Hou W, Zhong P, Chen L, Mai C, Qian Y, Zuo Y (2018a) Evaluating two optical methods of woody-to-total area ratio with destructive measurements at five *Larix gmelinii* Rupr. Forest plots in China. Forests 9:746. <https://doi.org/10.3390/f9120746>
- Zou J, Yan G, Chen L (2015) Estimation of canopy and woody components clumping indices at three mature *Picea crassifolia* forest stands. IEEE J Sel Top Appl Earth Obs Remote Sens 8:1413–1422. <https://doi.org/10.1109/JSTARS.2015.2418433>
- Zou J, Yan G, Zhu L, Zhang W (2009) Woody-to-total area ratio determination with a multispectral canopy imager. Tree Physiol 29:1069–1080. <https://doi.org/10.1093/treephys/tpp042>
- Zou J, Zhuang Y, Chianucci F, Mai C, Lin W, Leng P, Luo S, Yan B (2018b) Comparison of seven inversion models for estimating plant and woody area indices of leaf-on and leaf-off forest canopy using explicit 3D forest scenes. Remote Sens 10:1297. <https://doi.org/10.3390/rs10081297>
- Zou J, Zuo Y, Zhong P, Hou W, Leng P, Chen B (2019) Performance of four optical methods in estimating leaf area index at elementary sampling unit of *Larix principis-rupprechtii* forests. Forests 11:30. <https://doi.org/10.3390/f11010030>

Submit your manuscript to a SpringerOpen[®] journal and benefit from:

- Convenient online submission
- Rigorous peer review
- Open access: articles freely available online
- High visibility within the field
- Retaining the copyright to your article

Submit your next manuscript at ► [springeropen.com](https://www.springeropen.com)